Quantitative Radiomic Biomarkers for Discrimination Between Neuromyelitis Optica Spectrum Disorder and Multiple Sclerosis

Xiaoxiao Ma, MD,[1,2] Liwen Zhang, MD,[2,3] Dehui Huang, MD,[4] Jinhao Lyu, MD,[1] Mengjie Fang, MD,[2] Jianxing Hu, BS,[1] Yali Zang, PhD,[2] Dekang Zhang, BS,[1] Hang Shao,[5] Lin Ma, MD,[1] Jie Tian, PhD,[2*] Di Dong, PhD,[2*] and Xin Lou, MD[1*]

Background: Precise diagnosis and early appropriate treatment are of importance to reduce neuromyelitis optica spectrum disorder (NMOSD) and multiple sclerosis (MS) morbidity. Distinguishing NMOSD from MS based on clinical manifestations and neuroimaging remains challenging.
Purpose: To investigate radiomic signatures as potential imaging biomarkers for distinguishing NMOSD from MS, and to develop and validate a diagnostic radiomic-signature-based nomogram for individualized disease discrimination.
Study Type: Retrospective, cross-sectional study.
Subjects: Seventy-seven NMOSD patients and 73 MS patients.
Field Strength/Sequence: 3T/T_2-weighted imaging.
Assessment: Eighty-eight patients and 62 patients were respectively enrolled in the primary and validation cohorts. Quantitative radiomic features were automatically extracted from lesioned regions on T_2-weighted imaging. A least absolute shrinkage and selection operator analysis was used to reduce the dimensionality of features. Finally, we constructed a radiomic nomogram for disease discrimination.
Statistical Tests: Features were compared using the Mann–Whitney *U*-test with a nonnormal distribution. We depicted the nomogram on the basis of the results of the logistic regression using the rms package in R. The Hmisc package was used to investigate the performance of the nomogram via Harrell's C-index.
Results: A total of 273 quantitative radiomic features were extracted from lesions. A multivariable analysis selected 11 radiomic features and five clinical features to be included in the model. The radiomic signature ($P < 0.001$ for both the primary and validation cohorts) showed good potential for building a classification model for disease discrimination. The area under the receiver operating characteristic curve was 0.9880 for the training cohort and 0.9363 for the validation cohort. The nomogram exhibited good discrimination, a concordance index of 0.9363, and good calibration in the primary cohort. The nomogram showed similar discrimination, concordance (0.9940), and calibration in the validation cohort.
Data Conclusion: The diagnostic radiomic-signature-based nomogram has potential utility for individualized disease discrimination of NMOSD from MS in clinical practice.
Level of Evidence: 4
Technical Efficacy: Stage 2

J. MAGN. RESON. IMAGING 2019;49:1113–1121.

View this article online at wileyonlinelibrary.com. DOI: 10.1002/jmri.26287

Received Jun 28, 2018, Accepted for publication Jul 26, 2018.

*Address reprint requests to: X.L., Chinese PLA General Hospital, 28 Fuxing Road, Beijing, 100853, China. E-mail: louxin@301hospital.com.cn or D.D.,Institute of Automation, Chinese Academy of Sciences, Beijing 100190, China. E-mail: di.dong@ia.ac.cn; J.T., Institute of Automation, Chinese Academy of Sciences, Beijing 100190, China. E-mail: tian@ieee.org
The first two authors contributed equally to this work.

From the [1]Department of Radiology, Chinese PLA General Hospital, Beijing, China; [2]CAS Key Lab of Molecular Imaging, Institute of Automation, Chinese Academy of Sciences, Beijing, China; [3]University of Chinese Academy of Sciences, School of Artificial Intelligence, Beijing, China; [4]Department of Neurology, Chinese PLA General Hospital, Beijing, China; and [5]Automation Department, Tsinghua University, Beijing, China

Additional supporting information may be found in the online version of this article.

Neuromyelitis optica spectrum disorder (NMOSD) and multiple sclerosis (MS) are inflammatory demyelinating diseases of the central nervous system (CNS) that cause chronic neurological disability in early to middle adulthood.[1,2] Optic neuritis, myelitis, and brain involvement are common manifestations in both of these disorders.[3] Recent studies showed that NMOSD is an independent disease associated with aquaporin-4 antibody (AQP4-Ab) expression, rather than being a variant of MS.[4–7] Indeed, MS and NMOSD have divergent pathophysiologies, recommended treatment strategies for attack prevention, and prognoses.[8–12] Immunosuppressive agents, such as azathioprine, are the first-line treatment for NMOSD, whereas immunoregulatory agents, such as interferon beta (IFN-β), are recommended for the early treatment of MS.[9,13] Moreover, immunotherapies for MS appear to exacerbate NMOSD; IFN-β is thought to be ineffective or even harmful in patients with NMOSD.[13,14] Thus, the precise diagnosis and early appropriate treatment are crucial for reducing MS and NMOSD morbidity.[9,10,14]

Laboratory findings such as serum AQP4-Ab levels have been widely applied in clinical practice and medical research to discriminate NMOSD from MS.[9,10,13,15] However, a portion of NMOSD cases are AQP4-Ab negative, and a minority of MS patients are AQP4-Ab positive.[16] Magnetic resonance imaging (MRI) is also routinely employed for the screening, diagnosis, evaluation, and monitoring of patients with NMOSD or MS. However, conventional MRI interpretation is limited by using subjective and qualitative imaging descriptors such as signal characteristics, lesion distribution, and morphology, while advanced imaging modalities such as iron-deposition imaging only provide a single or a few markers.[17] Even with the currently available diagnostic tools, distinguishing NMOSD from MS based on clinical manifestations and neuroimaging remains a significant challenge, especially for NMOSD cases with multiple brain lesions resembling MS.[4,15,18–20]

In recent years, radiomics has emerged as an intelligent technique for medical imaging analysis. Radiomics is a process of extracting quantitative features from digital medical images and combining relevant clinical variables to develop a scientific and largely data-driven analysis model.[21–23] Compared to individual analyses, radiomics provides better grounds for medical decisions. Previous studies have demonstrated that, in addition to being correlated with gene expression patterns, radiomic features are of great significance to distant metastasis prediction and prognosis in patients with various malignancies such as intrahepatic cholangiocarcinoma, glioblastoma, and colorectal cancer.[24–26] However, research using radiomics for the diagnosis of demyelinating CNS diseases is limited. The primary goal of the present study was to investigate whether radiomic features could be used to distinguish NMOSD from MS, and to develop and validate a radiomic-signature-based diagnostic nomogram for individualized disease discrimination in patients with these disorders.

Materials and Methods

Ethics Statement

The study was approved by the Ethics Committee of our hospital and all patients provided written informed consent prior to study participation.

Subjects

We enrolled 150 patients in our study. For the primary cohort, 47 patients who had received a diagnosis of NMOSD and 41 patients who had received a diagnosis of MS from January 2012 to December 2015 were retrospectively enrolled. An additional 30 patients who had received a diagnosis of NMOSD and 32 patients who had received a diagnosis of MS from November 2015 to March 2017 were retrospectively included in the validation cohort. The inclusion criterion was: a diagnosis of MS as per the 2010 revision of the McDonald criteria[27] or a diagnosis of NMOSD as per the 2015 international consensus diagnostic criteria.[5] The exclusion criteria were: 1) intravenous corticosteroid treatment in the last 30 days prior to imaging; 2) a clinical relapse in the last 3 months prior to imaging; 3) contraindications for MRI such as claustrophobia; 4) poor image quality or large motion artifacts; 5) other neurodegenerative diseases, metabolic disorders, or cerebrovascular diseases; 6) recent use of antidepressant medication; 7) alcoholism; or 8) psychological disorders, except for depression as per the Diagnostic and Statistical Manual of Mental Disorders, 4th edition, diagnostic guidelines.

Baseline demographic and laboratory data including age, gender, current treatment, AQP4-Ab status, oligoclonal band (OCB), diagnosis, and clinical status (relapse or remission) were assessed independently by two neurologists, each with more than 10 years of experience. Disagreements between the two specialists were resolved by discussion and consensus. Serum AQP4-Ab levels were determined using an indirect immunofluorescence kit (EUROIMMUN Medizinische Labor Diagnostika, Lübeck, Germany) in accordance with the manufacturer's guidelines after diluting the serum samples 1:9. For OCB detection, 2 mL of cerebrospinal fluid (CSF) was obtained by lumbar puncture. OCB was detected by isoelectric focusing on a polyacrylamide gel followed by immunoblotting. Two or more bands indicated OCB positivity.

MRI Protocol

Whole-brain imaging was performed on a 3.0T scanner (GE Discovery MR 750, GE Healthcare, Milwaukee, WI). The MRI protocol included axial T_2-weighted (T_2WI), coronal T_2 fluid attenuation inversion recovery (FLAIR), axial T_1-weighted (T_1WI), and matching T_1-weighted postcontrast imaging. The following scan parameters were used. Axial T_2WI: repetition time (TR) = 6829 msec, echo time (TE) = 93 msec, echo train length (ETL) = 32, slice number = 24, slice thickness = 5.0 mm, field of view (FOV) = 24 × 24 cm, matrix size = 512 × 512; coronal T_2 FLAIR: TR = 8500 msec, TE = 162 msec, ETL = 40, slice number = 24, slice thickness = 5.0 mm, FOV = 24 × 24 cm, matrix size = 288 × 224; axial T_1WI: TR = 1850 msec, TE = 24 msec, ETL = 10, slice number = 24, slice thickness = 5.0 mm, FOV = 24 × 24 cm, matrix size = 320 × 320).

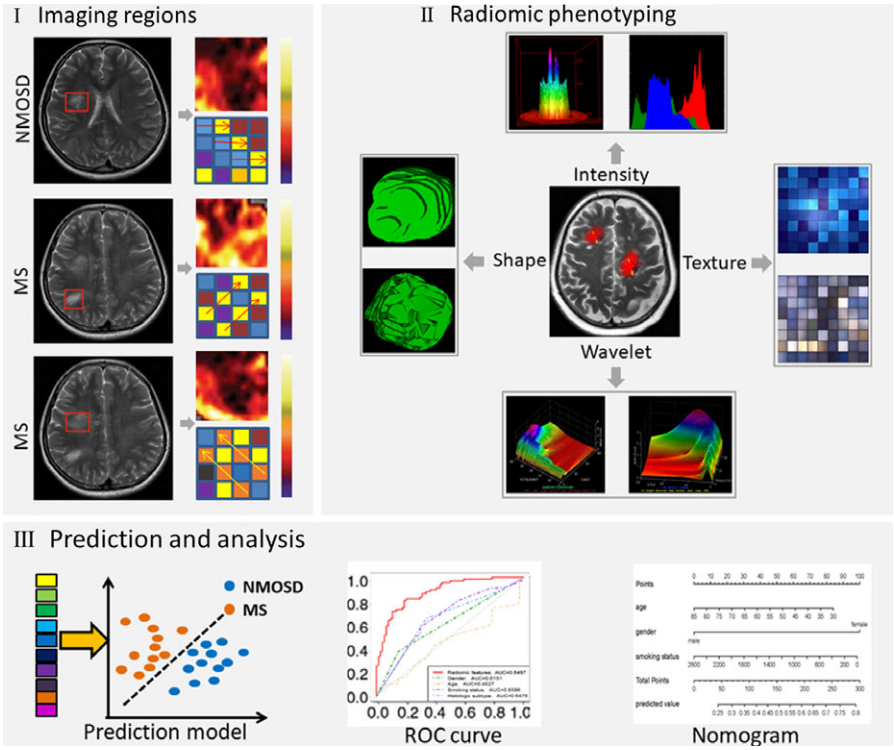

FIGURE 1: Radiomic analyses. (I) Original region selection and phenotypes from three patient ROIs. Patient labels are shown on the left. (II) Extraction of features from ROIs, such as lesion shape, intensity, texture, and wavelet features. (III) Prediction and analysis. MS, multiple sclerosis; NMOSD, neuromyelitis optica spectrum disorder; ROC, receiver operating curve.

Lesion Delineation and Selection

MS and NMOSD lesions were manually segmented on axial T_2WI projections to obtain regions of interest (ROIs) with the ITK-SNAP software (open-source software; www.itk-snap.org). Segmentation was completed by a radiologist with more than 5 years of experience (X.L.) and validated by another radiologist with 2 years of experience (X.X.M.). Lesions were selected if the lesion diameter was greater than 3 mm in the slice with the largest cross-section, and if the lesion was in the periventricular, juxtacortical, or infratentorial regions, or the subcortical white or deep gray matter.[28] Axial T_1WI and coronal T_2 FLAIR imaging were used to identify and delineate lesions. Only lesions presented on all three sequences were selected to reduce the possibility of misidentification. When a lesion was large and presented at multiple slices, we drew a ROI for one lesion at a single slice with the largest cross-section. T_1-weighted postcontrast imaging was used to assist neurologists in evaluating the clinical status of the patients.

For each patient, we delineated several ROIs and checked them to ensure that a patient only had NMOSD or MS at the same time and each ROI belonged to one group. Therefore, an MS or NMOSD patient had many ROIs and we designated each ROI as an individual case to increase the amount of data.

Radiomic Feature Extraction and Selection

We quantified imaging phenotype by radiomic features extracted from each ROI; the visualized process of the radiomic approach is shown as Fig. 1.[23] To read easily, we described the radiomic features with more detailed information in the Supplementary Materials. To ensure the stability of radiomic features against delineation inaccuracies, 30 patients were randomly selected from the entire sample, and another radiologist, with 5 years of experience in the study of inflammatory demyelinating diseases, delineated lesion ROIs, which were used to calculated interobserver correlation coefficients (ICCs) to evaluate the reliability and validity of all radiomic features.[29] The least absolute shrinkage and selection operator (LASSO) method was applied to select certain representative features,[30] and the selected features were used to build radiomic signature and calculate radiomic score (Rad-score) for each patient. Most of the covariate coefficients were reduced to zero, and the remaining nonzero coefficients were selected. The formula of the model constructed by the nonzero coefficient of selected features was defined as the Rad-score. A radiomic signature (the output value of Rad-score) was built in the primary and validation cohorts.

Visualized Nomogram Analysis

Neurologists and patients want to have reliable discriminative tools that are tailored to the individual patient. A radiomic nomogram with user-friendly graphical interfaces was created to visualize a multivariable logistic regression model predictive of differential diagnosis between NMOSD and MS with the following representative predictors: gender, AQP4-Ab, OCB, spinal lesions, and radiomic signature.[26,31]

Calibration Curves of the Radiomic Nomogram

We built the radiomic nomogram on the basis of a multivariable logistic analysis of the primary cohort. To assess nomogram calibration, we plotted calibration curves of the radiomic nomogram for the primary and validation cohorts. Crossvalidation was performed using the patient datasets. The performance of the validated nomogram was tested in the validation cohort. The logistic regression

TABLE 1. Analysis of Patient Characteristics in the Primary and Validation Cohorts

Characteristic	Primary cohort			Validation cohort		
	MS	NMOSD	*P*	MS	NMOSD	*P*
No. of patients	41	47	—	32	30	—
Regions	361	354	—	218	186	—
Age (mean ± SD), years	33.9 ± 10.5	35.4 ± 14.2	0.005	38.9 ± 9.3	38.5 ± 15.4	<0 .001
Gender			<0 .001			< 0.001
Male	16 (39%)	2 (4%)		10 (31%)	6 (20%)	
Female	25 (61%)	45 (96%)		22 (69%)	24 (80%)	
AQP4-Ab			<0 .001			< 0.001
Positive (+)	0 (0%)	37 (79%)		0 (0%)	19 (63%)	
Negative (–)	41 (100%)	10 (21%)		32 (100%)	11 (37%)	
OCB			<0 .001			0.021
Positive (+)	32 (78%)	12 (26%)		20 (63%)	12 (40%)	
Negative (–)	9 (22%)	34 (72%)		5 (16%)	13 (43%)	
Unknown	0 (0%)	1 (2%)		7 (21%)	5 (17%)	
Spinal lesions			0.015			0.222
Positive (++)	6 (14%)	16 (34%)		8 (25%)	16 (53%)	
Positive (+)	13 (32%)	15 (32%)		9 (28%)	9 (30%)	
Negative (–)	22 (54%)	16 (34%)		15 (47%)	5 (17%)	
Rad-score (mean)	2.241	−3.120	<0 .001	14.806	0.860	<0 .001

For spinal lesions, positive (++) represents longitudinally extensive lesions involving ≥3 vertebral segments, positive (+) represents lesions involving < 3 vertebral segments, and negative (–) represents absence of lesions. AQP4-Ab, aquaporin-4 antibody; MS, multiple sclerosis; NMOSD, neuromyelitis optica spectrum disorder; OCB, oligoclonal band; Rad-score, radiomic score; SD, standard deviation.

formula derived from the primary cohort was applied to the validation cohort and total point was calculated for each patient.

Statistical Analyses

Feature extraction was performed using MATLAB 2015b (MathWorks, Natick, MA), and statistical analyses were performed with the R software (v. 3.3.3; http://www.R-project.org). The SPM12 package was implemented in MATLAB 2015b to read original images. Representative features were selected from 273 features using the glmnet package. Features were compared using the Mann–Whitney *U*-test with a nonnormal distribution.[32] The prediction model was developed using a binary logistic regression analysis. We depicted the nomogram on the basis of the results of the logistic regression using the rms package in R. The Hmisc package was used to investigate the performance of the nomogram via Harrell's C-index.[33] The range of the C-index is from 0.5 to 1.0, with the highest value (C-index = 1) indicates a perfect ability to show no difference between the real value of the model and the predicted value. Bootstrap analyses with 1000 resamples were used to obtain C-index statistics that were corrected for potential overfitting. $P < 0.05$ was considered to be statistically significant.

Results

Clinical Data Analysis

Clinical characteristics of patients for the primary and validation cohorts are shown as Table 1. We found no significant differences between the cohorts ($P > 0.81$) in age, gender, AQP4-Ab, OCB, spinal lesions, or Rad-score.

Feature Extraction and Selection

We delineated a total of 1119 ROIs in 150 patients and extracted 273 radiomic features from each ROI. The primary cohort consisted of 715 regions in 88 patients, and the validation cohort consisted of 404 regions in 62 patients (Table 1). Significant clinical variables included age, gender, AQP4-Ab, OCB, and spinal lesions ($P < 0.05$ for all). Ten-fold crossvalidation was performed for LASSO regression analysis. Finally,

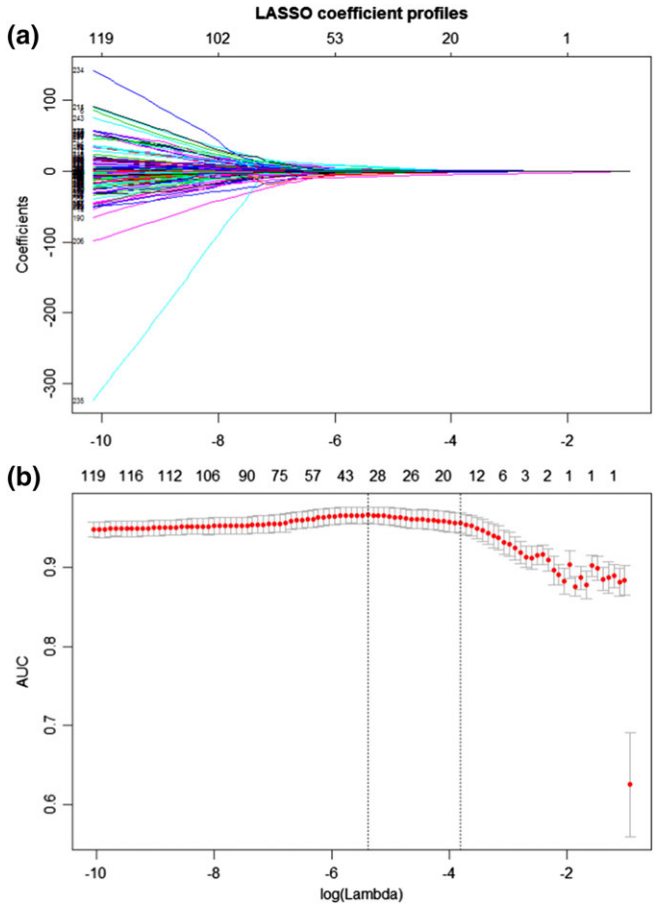

FIGURE 2: LASSO binary logistic regression model for feature selection. a: With the number of coefficients of the 273 radiomic features and five clinical variables shrinking, the value of In(Lambda) increased. The optimal value of Lambda was 0.022, and the value of In(Lambda) was –3.817. The vertical dotted line represents the value selected by 10-fold crossvalidation, where 16 optimal coefficients were obtained. **b**: The relationship between the AUC and the parameter is shown. When In(Lambda) increased to –3.817, the AUC peaked again with the appropriate number of features as per the 10-fold crossvalidation. X-axes represent the dynamic change of the tuning parameter of Lambda for the LASSO feature selection.

16 potential predictors were used to develop a LASSO logistic regression model (Fig. 2). Cronbach's α values of 0.7–0.8 are considered satisfactory for ICC-based evaluation of the reliability and validity of radiomic features. In our test of feature reliability, Cronbach's α for interobserver agreement was 0.927.

Development of the Prediction Model and ROC Curve Analysis

The LASSO logistic regression analysis indicated that 11 radiomic features combined with five clinical features could potentially be used to build a prediction model. More information on the model can be found in the Supplementary Materials (eTables 1–4).

We evaluated the performances of each clinical feature (Fig. 3a): age (AUC = 0.5867), gender (AUC = 0.7501), AQP4-Ab (AUC = 0.8815), OCB (AUC = 0.7313), and spinal lesions (AUC = 0.4754). A model incorporating these clinical features (AUC = 0.8206) showed similar performance with radiomic features (AUC = 0.8212) in the validation cohort. Moreover, the model combining both clinical features and radiomic features showed the best performance for the discrimination (AUC in primary cohort: 0.9880; AUC in validation cohort: 0.9363).

Development of an Individualized Nomogram

We found that gender ($P < 0.001$), AQP4-Ab ($P < 0.001$), OCB ($P < 0.001$), spinal lesions ($P = 0.015$), and radiomic signature ($P < 0.001$) as independent differentiators between NMSOD and MS by logistic regression analysis. An individualized NMOSD/MS prediction model consisting of the aforementioned independent predictors was visualized as a nomogram (Fig. 4a). The nomogram showed good discrimination performance between NMSOD and MS (C-index: 0.9363, 95% confidence interval [CI]: 0.9826–0.9942).

Validation of the Radiomic Nomogram With Calibration Curves

We plotted calibration curves to validate the performance of the nomogram in the primary cohort with the Hosmer-Lemeshow test (Fig. 4b). We calculated Harrell's C-index and 1000 bootstrap resamples for validation. The calibrated C-index was 0.9940 (95% CI: 0.990–0.997; Fig. 4c).

Discussion

In the present study, we investigated the ability of radiomic features extracted from conventional MRI to accurately distinguish NMOSD from MS. A radiomic signature assembled from 11 differentiation-associated features showed good potential as a biomarker for distinguishing the two disorders in the primary and validation cohorts. When combined with related clinical characteristics, the radiomic signature exhibited excellent discriminative performance. We used these results to develop a radiomic-signature-based nomogram for individualized discrimination in patients with NMOSD or MS.

We studied a total of 273 radiomic features extracted from T_2WI projections, including semantic, intensity, texture, and wavelet features. The 11 radiomic features, identified by shrinking the regression coefficients with the LASSO method, were selected for a radiomic signature. A multivariable logistic regression analysis demonstrated a diagnostic accuracy of the radiomic signature comparable to the clinical method of AQP4-Ab, which is routinely used in clinical settings to distinguish NMOSD from MS.[9,10,13] We found that the application of radiomics on traditional T_2WI is noninvasive, feasible, cost-efficient, reproducible, and comparable with AQP4-Ab. Combining radiomics with the key variables (age, gender, AQP4-Ab, OCB, and spinal lesions) improved

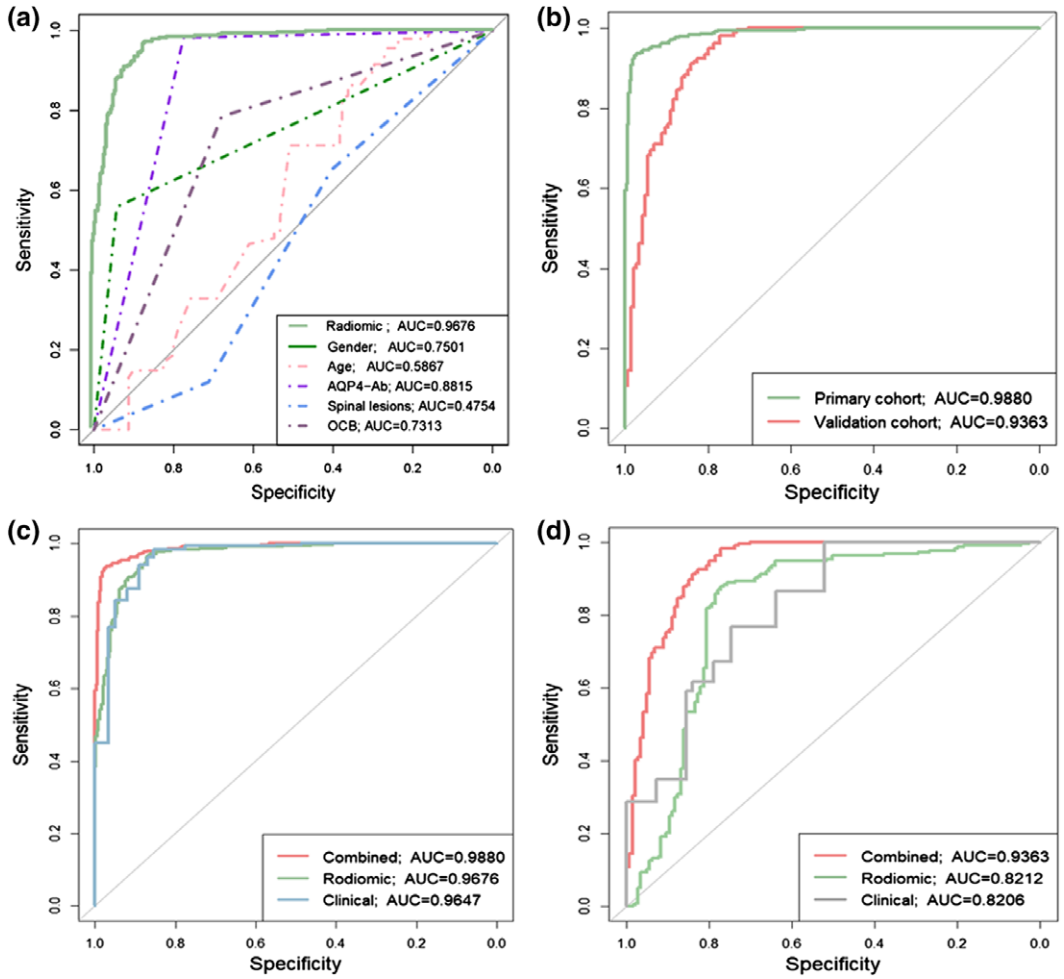

FIGURE 3: ROC analysis. **a**: ROC curves were plotted to describe the clinical variables. Each curve represents a model built for the indicated variable. **b**: ROC curves for the primary and validation cohorts. **c**: ROC curves plotted for radiomic features, clinical features, or both showed good discriminative performance in the primary cohort. **d**: ROC curves were plotted for radiomic features, clinical features, or both to differentiate MS from NMOSD in the validation cohort.

its differentiation accuracy in the primary and validation cohorts. Therefore, the proposed model is promising and appealing for clinical decision support in patients with NMOSD or atypical MS.

Although diagnosis criteria are accepted and acknowledged by most neurologists, NMOSD and MS are still hard to differentiate by experienced experts from visual inspection of imaging. Subtle structural and pathological differences between NMOSD and MS have been reported.[4,8,34,35] For example, MS presented a varying extent of inflammation, axonal loss, oligodendrocyte injury, gliosis, neurodegeneration, microglia, and macrophage infiltration, while NMOSD showed a perivascular deposition of immunoglobulin and complement activation.[1,11] Most MS lesions were traversed by the central venule and extended along it, whereas few NMOSD lesions involved the central venule.[4,34,35] About 23% of MS lesions had a clear hypointense rim that was rarely detected in NMOSD lesions.[8] Iron metabolism resulting from iron-rich macrophages, microglia or oligodendrocytes, perivascular hemoglobin leakage, or a loss of diamagnetic myelin was more frequently detected in MS than in NMOSD lesions.[8] Differences in the extent of tissue injury may cause alterations in the distribution pattern of MRI intensity which unfortunately are indistinguishable by conventional imaging interpretation.[36]

A previous study demonstrated that texture analysis may be useful to reflect the subtle tissue-level features, in line with pathological findings.[36] It was reported that texture heterogeneity was associated with the severity of tissue pathological damage.[36] The texture feature of GLRLM_GLN measures the similarity of gray level values throughout the ROI. If the gray level values are similar, the value is small. In our study we found that patients with MS had a smaller GLRLM_GLN value than NMOSD, which may reflect that more severe tissue damage existed in patients with NMOSD than MS. Besides textural features, radiomics is able to extract other types of features from medical images. We also found that several wavelet features were significantly different between the two diseases. Further investigations are necessary to verify and confirm the findings between radiomic features

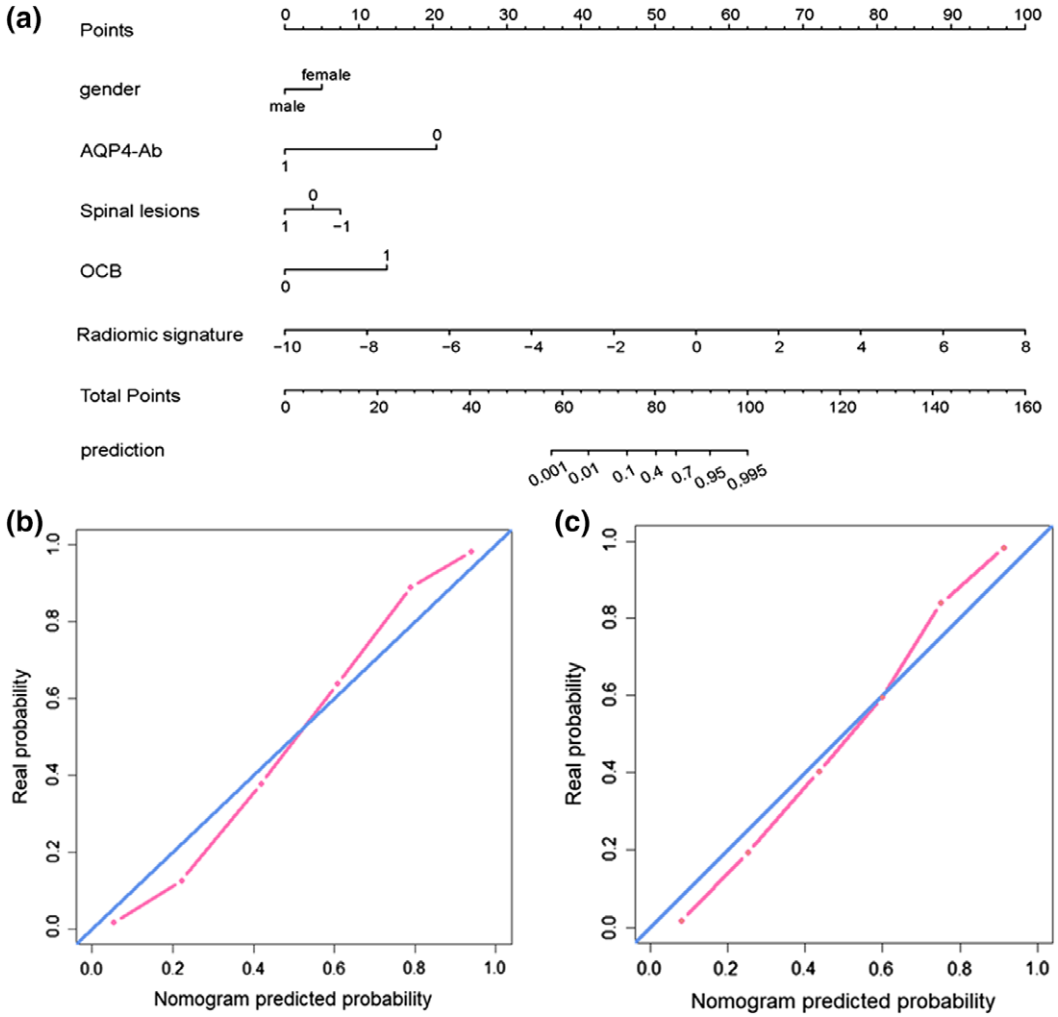

FIGURE 4: Construction of radiomic nomogram and calibration. a: The nomogram was generated to depict the potential predictive ability of the model for each patient in the primary cohort, incorporating gender, aquaporin-4 antibody (AQP4-Ab), spinal lesions (1, more than 3 spinal segments; –1, less than 3 spinal segments; 0, no lesions), oligoclonal band (OCB), and radiomic signature (Rad_signature). **b**: Calibration curve of the radiomic nomogram in the primary cohort. **c**: Calibration curve of the radiomic nomogram in the validation cohort. X-axes represent the nomogram-predicted probability. Y-axes represent the actual probability. The blue diagonal line shows an ideal prediction by an optimal model, and the pink line shows the calibrated values of the nomogram. The calibration curve was drawn by plotting P1 on the X-axis and P2 = [1+exp-(x1+ax2)]-1 on the Y-axis, where P2 is the real probability, a = logit (P1), P1 is the predicted probability, x1 is the calibration intercept, and x2 is the estimated slope.

and pathophysiological changes, and facilitate our intelligent diagnosis model into clinical application.

Although the spinal lesions alone were insufficient to separate NMOSD from MS, as revealed in the multivariable logistic regression, they were important markers in the diagnosis of NMOSD or MS. The presence of longitudinally extensive spinal cord lesions (involving ≥3 vertebral segments) that preferentially affect spinal central gray matter is a typical characteristic of NMOSD, whereas other lesion types are indicative of MS.[37] Iasonos et al proposed that the range of variables utilized in nomograms was determined by data availability and clinical evidence rather than statistical significance.[31] Therefore, spinal lesions should be considered an important differentiating NMOSD/MS biomarker.

In our study, we built a nomogram that combined the radiomic signature with the representative clinical factors (gender, AQP4-Ab, OCB, and spinal lesions), which exhibited good performance in individualized discrimination for patients with MS and NMOSD. The nomogram would facilitate our diagnosis model into clinical practice.

The present study has several important limitations. The major limitation was that although a series of radiomic features were identified to differentiate NMOSD from MS, the underlying pathological indication of a specific feature was not clear and not correlated with clinical manifestations. Second, we enlarged the patient size by the method that we designated each ROI as an individual case, which may influence the statistics analysis for the significance of clinical features. Further work should follow this method. Third, optic neuropathy graphics were not obtained to support the differentiation, although involving of optic nerve could be different in NMOSD and MS.[38] Fourth, radiomic analysis was

performed on T_2WI alone and in 2D images. The reason was that in our routine head protocol, T_2WI had the highest axial spatial resolution, which would promote the efficiency of ROI delineation and partial volume effect reduction. In a future study we will enroll more sequences, such as T_1WI, double inversion recovery FLAIR, and susceptibility-weighted imaging (SWI), to improve our radiomic nomogram. Fifth, the cohorts did not cover the spectrum of MS and NMOSD, since all patients were in the chronic stage of the disease and MS patients were all of the relapsing-remitting type, which may induce bias in implementing the results into practice. Sixth, despite the long study period, the sample size was relatively small.

In conclusion, we established and validated a radiomic nomogram incorporating radiomic signature and clinical characteristics which can be used to provide increased diagnostic accuracy in distinguishing NMOSD from MS. Future studies are required to validate the generalizability of our integrated nomogram for individualized discrimination in patients with NMOSD or MS.

Acknowledgment

Contract grant sponsor: National Natural Science Foundation of China; Contract grant numbers: 81227901, 61231004, 81771924, 81501616, 81671126, 81730048; Contract grant sponsor: Special Program for Science and Technology Development from the Ministry of Science and Technology, China; Contract grant numbers: 2017YFA0205200, 2017YFC1308701, 2017YFC1309100, 2016CZYD0001, 2016YFC0100104; Contract grant sponsor: Science and Technology Service Network Initiative of the Chinese Academy of Sciences; Contract grant number: KFJ-SW-STS-160.

References

1. Lucchinetti CF, Mandler RN, McGavern D, et al. A role for humoral mechanisms in the pathogenesis of Devic's neuromyelitis optica. Brain 2002; 125:1450–1461.
2. Isobe N, Keshavan A, Gourraud PA, et al. Association of HLA genetic risk burden with disease phenotypes in multiple sclerosis. JAMA Neurol 2016;73:795–802.
3. Huh SY, Min JH, Kim W, et al. The usefulness of brain MRI at onset in the differentiation of multiple sclerosis and seropositive neuromyelitis optica spectrum disorders. Mult Scler 2014;20:695–704.
4. Sinnecker T, Dorr J, Pfueller CF, et al. Distinct lesion morphology at 7-T MRI differentiates neuromyelitis optica from multiple sclerosis. Neurology 2012;79:708–714.
5. Wingerchuk DM, Banwell B, Bennett JL, et al. International consensus diagnostic criteria for neuromyelitis optica spectrum disorders. Neurology 2015;85:177–189.
6. Liu Y, Duan Y, Huang J, et al. Multimodal quantitative MR imaging of the thalamus in multiple sclerosis and neuromyelitis optica. Radiology 2015; 277:784–792.
7. Jurynczyk M, Craner M, Palace J. Overlapping CNS inflammatory diseases: differentiating features of NMO and MS. J Neurol Neurosurg Psychiatry 2015;86:20–25.
8. Sinnecker T, Schumacher S, Mueller K, et al. MRI phase changes in multiple sclerosis vs neuromyelitis optica lesions at 7T. Neurol Neuroimmunol Neuroinflamm 2016;3:e259.
9. Lennon VA, Wingerchuk DM, Kryzer TJ, et al. A serum autoantibody marker of neuromyelitis optica: distinction from multiple sclerosis. Lancet 2004;364:2106–2112.
10. Chawla S, Kister I, Wuerfel J, et al. Iron and non-iron-related characteristics of multiple sclerosis and neuromyelitis optica lesions at 7T MRI. AJNR Am J Neuroradiol 2016;37:1223–1230.
11. Popescu BF, Pirko I, Lucchinetti CF. Pathology of multiple sclerosis: where do we stand? Continuum 2013;19:901–921.
12. Wegner C. Recent insights into the pathology of multiple sclerosis and neuromyelitis optica. Clin Neurol Neurosurg 2013;115(Suppl 1): S38–41.
13. Jarius S, Wildemann B. Aquaporin-4 antibodies (NMO-IgG) as a serological marker of neuromyelitis optica: a critical review of the literature. Brain Pathol 2013;23:661–683.
14. Palace J, Leite MI, Nairne A, Vincent A. Interferon Beta treatment in neuromyelitis optica: increase in relapses and aquaporin 4 antibody titers. Arch Neurol 2010;67:1016–1017.
15. Eshaghi A, Riyahi-Alam S, Saeedi R, et al. Classification algorithms with multi-modal data fusion could accurately distinguish neuromyelitis optica from multiple sclerosis. Neuroimage Clin 2015;7: 306–314.
16. Calabrese M, Oh MS, Favaretto A, et al. No MRI evidence of cortical lesions in neuromyelitis optica. Neurology 2012;79: 1671–1676.
17. Chen X, Zeng C, Luo, T, et al. Iron deposition of the deep grey matter in patients with multiple sclerosis and neuromyelitis optica: A control quantitative study by 3D-enhanced susceptibility-weighted angiography (ESWAN). Eur J Radiol 2012;81:e633–e639.
18. Ciccarelli O, Thomas DL, De Vita E, et al. Low myo-inositol indicating astrocytic damage in a case series of neuromyelitis optica. Ann Neurol 2013;74:301–305.
19. Tallantyre EC, Morgan PS, Dixon JE, et al. A comparison of 3T and 7T in the detection of small parenchymal veins within MS lesions. Invest Radiol 2009;44:491–494.
20. Duan Y, Liu Y, Liang P, et al. Comparison of grey matter atrophy between patients with neuromyelitis optica and multiple sclerosis: a voxel-based morphometry study. Eur J Radiol 2012;81:e110–114.
21. Lambin P, Rios-Velazquez E, Leijenaar R, et al. Radiomics: extracting more information from medical images using advanced feature analysis. Eur J Cancer 2012;48:441–446.
22. Gillies RJ, Kinahan PE, Hricak H. Radiomics: images are more than pictures, they are data. Radiology 2016;278:563–577.
23. Aerts HJWL, Velazquez ER, Leijenaar RTH, et al. Decoding tumour phenotype by noninvasive imaging using a quantitative radiomics approach. Nat Commun 2014;5:4006.
24. Wang Y, Li J, Xia Y, et al. Prognostic nomogram for intrahepatic cholangiocarcinoma after partial hepatectomy. J Clin Oncol 2013;31: 1188–1195.
25. Korfiatis P, Kline TL, Coufalova L, et al. MRI texture features as biomarkers to predict MGMT methylation status in glioblastomas. Med Phys 2016;43:2835–2844.
26. Huang YQ, Liang CH, He L, et al. Development and validation of a radiomics nomogram for preoperative prediction of lymph node metastasis in colorectal cancer. J Clin Oncol 2016;34:2157–2164.
27. Polman CH, Reingold SC, Banwell B, et al. Diagnostic criteria for multiple sclerosis: 2010 revisions to the McDonald criteria. Ann Neurol 2011;69: 292–302.
28. Cramer SP, Simonsen H, Frederiksen JL, Rostrup E, Larsson HB. Abnormal blood-brain barrier permeability in normal appearing white matter in multiple sclerosis investigated by MRI. Neuroimage Clin 2014;4: 182–189.

29. Weir JP. Quantifying test-retest reliability using the intraclass correlation coefficient and the SEM. J Strength Cond Res 2005;19:231–240.

30. Tibshirani R. Regression selection and shrinkage via the Lasso. J R Stat Soc B 1996;58:267–288.

31. Iasonos A, Schrag D, Raj GV, Panageas KS. How to build and interpret a nomogram for cancer prognosis. J Clin Oncol 2008;26:1364–1370.

32. Ruxton GD. The unequal variance t-test is an underused alternative to Student's t-test and the Mann-Whitney U test. Behav Ecol 2006;17: 688–690.

33. Koziol JA, Jia Z. The concordance index C and the Mann-Whitney parameter Pr (X> Y) with randomly censored data. Biometr J 2009;51: 467–474.

34. Ge Y, Zohrabian VM, Grossman RI. Seven-tesla magnetic resonance imaging: new vision of microvascular abnormalities in multiple sclerosis. Arch Neurol 2008;65:812–816.

35. Kister I, Herbert J, Zhou Y, Ge Y. Ultrahigh-field MR (7 T) imaging of brain lesions in neuromyelitis optica. Mult Scler Int 2013;2013:398259.

36. Zhang Y, Moore GR, Laule C, et al. Pathological correlates of magnetic resonance imaging texture heterogeneity in multiple sclerosis. Ann Neurol 2013;74:91–99.

37. Barnett Y, Sutton IJ, Ghadiri M, Masters L, Zivadinov R, Barnett MH. Conventional and advanced imaging in neuromyelitis optica. AJNR Am J Neuroradiol 2014;35:1458–1466.

38. Kim H, Paul F, Lana-Peixoto M, et al. MRI characteristics of neuromyelitis optica spectrum disorder. Neurology 2015;84:1165–1173.